METHODS*: FIELD SAMPLING*

I. Locality Information

Confusion Range, Utah:

GPS coordinates: 12 S 268459 4366086

Reference(s):
Carr, T., 1981, Paleogeography, depositional history, and conodont paleoecology of the Lower Triassic Thaynes Formation in the Cordilleran Miogeosyncline, Unpublished PhD, University of Wisconsin-Madison.

Collinson, J.W., Kendall, C.G.St.C., and Marcantel, J.B., 1976, Permian-Triassic boundary in eastern Nevada and west-central Utah: Geological Society of America Bulletin, v. 87, p. 821-824.

Hose, R. K., and C. A. Repenning, 1959, Stratigraphy of Pennsylvanian, Permian, and Lower Triassic rocks of Confusion Range, west-central Utah: AAPG Bull., v. 43, p. 2167-2196.

Hose, R. K., and C. A. Repenning, 1963, Geologic map and sections of the 1956. Cowboy Pass NW quadrangle. Confusion Range, Millard County, Utah: U.S. Geol. Survey Misc. Geol. Inv. Map 1-378, scale 1:24,000.

Stephen, D.A., Bylund, K.G., Bybee, P.J., Ream, W.J., 2008, Lower Triassic ammonoid beds in the Confusion Range of western Utah, Geological Society of America *Abstracts with Programs*, Vol. 40, No. 1, p. 59, Cordilleran Section (104th Annual) and Rocky Mountain Section (60th Annual) Joint Meeting (19–21 March 2008)

Spruce Mountain, Nevada:

GPS coordinates: 11 T 694518 4484956

Reference:
Carr, T., 1981, Paleogeography, depositional history, and conodont paleoecology of the Lower Triassic Thaynes Formation in the Cordilleran Miogeosyncline, Unpublished PhD, University of Wisconsin-Madison. "**Spruce Mountain**" section.

Nearby sections (these are referred to as Southern Pequop Mountains, and north of Currie, NV, which are within about 5-15km of Spruce Mountain):

Collinson, J.W., Kendall, C.G.St.C., and Marcantel, J.B., 1976, Permian-Triassic boundary in eastern Nevada and west-central Utah: Geological Society of America Bulletin, v. 87, p. 821-824.

Lucas, S.G. and Orchard, M.J., 2007, Triassic lithostratigraphy and biostratigraphy north of Currie, Elko County, Nevada, In Lucas, S.G. and Spielmann, J.A., eds. 2007, Triassic of the American West: New Mexico Museum of Natural History and Science Bulletin 40, p. 119-126.

II. Construction of Confusion Range – Spruce Mountain Composite Section

In the Confusion Range section of western Utah, the entire Gerster Formation is preserved up through the lowermost Thaynes (see stratigraphic columns in Figures 1 and 2 of the paper). Above the lowermost Thaynes, a stream bed and presumed faulting interrupts the continuity of the section. Because we felt it was important to document the $\delta^{13}C$ curve from younger parts of the Thaynes to provide additional tie points for correlations with Tethyan sections, we sought a suitable alternative to the Confusion Range. The section at Spruce Mountain in Nevada was determined to provide the best combination of biostratigraphic control and exposure (Carr, 1981). Although the Spruce Mountain section contains a long covered interval in the Thaynes, in our experience this was nonetheless the best exposure in the region and therefore was used for construction of a composite $\delta^{13}C$ curve to make comparisons with the Early Triassic of the Tethys. We visited sections A and B of Lucas and Orchard (2007), but did not produce detailed isotope curves there. Nonetheless, it is important to emphasize that we found no rocks in these sections that appeared to correlate lithologically or chemostratigraphically with the portion of the Confusion Range section, where our isotope curves indicate likely preservation of the Permo-Triassic boundary interval (i.e., the upper portion of the Gerster Fm in Fig 2 in manuscript). This is consistent with the conclusions of Lucas and Orchard (2007).

Correlation of the Confusion Range and Spruce Mountain sections to make the composite used the first appearance of the brown, ammonite-bearing beds that are used to define the base of the Thaynes regionally. These beds occur in both the Confusion Range and Spruce Mountain sections and have been dated as Smithian using conodonts and ammonites (Collinson et al., 1976; Carr, 1981; Lucas and Orchard, 2007; Stephen et al., 2008). The $\delta^{13}C$ and $^{87}Sr/^{86}Sr$ values for the traditional brown, ammonite-bearing basal Thaynes beds at both sections are indistinguishable (at about -3 to -4 ‰ for C and ~ 0.7080 for Sr) and support construction of the composite as shown in Figure 1, in which about 3.5 meters of basal Thaynes from Spruce Mountain are placed above the fenestral, laminated and microgastropod limestone beds included in the topmost "Gerster" at the Confusion Range section that are atypical of the Gerster or Thaynes at Spruce Mountain. Note that a small amount of overlap between sections cannot be ruled out within the resolution provided by both conodonts and $\delta^{13}C$ values, but does not affect the main

conclusions of this paper that focus on where our isotope curves indicate may be the Permo-Triassic boundary interval in the Confusion Range in the upper portion of the Gerster Fm (Fig 2 in manuscript). We have no evidence that rocks correlative to what we describe in the Confusion Range Gerster-Thaynes transition interval are exposed in Spruce Mountain/Currie area, consistent with a hiatus at Spruce Mountain as indicated by Lucas and Orchard (2007).

METHODS: *ANALYTICAL*

For carbonate samples collected in the field, all weathered surfaces were removed and samples were sonicated with deionized water to remove loose sediment. A drill with a 1 mm bit was used to obtain carbonate powder from slabs. Homogeneous micritic limestone was the preferred component, although many of the sampled phases isolated (~40 mg of powder) had a coarser-grained component that had been recrystallized to various degrees. Secondary veins were avoided in drilling.

I. Carbon Isotope Analytical Methods

Carbonate powders were roasted in a vacuum oven at 200°C for 1 hour to remove water and volatile organic contaminants. 10-50 micrograms of carbonate were reacted at 70°C with 3-5 drops of anhydrous phosphoric acid for 180-300 seconds. Stable isotope values were obtained using a Finnigan Kiel-III carbonate preparation device directly coupled to the dual inlet of a Finnigan MAT 253 isotope ratio mass spectrometer at Ohio State University and the University of Kansas stable isotope facilities. The analytical precision based on duplicate analyses and on multiple analyses of NBS19 was $\leq 0.04‰$.

II. Strontium Isotope Analytical Methods

Procedures based on work by Montañez et al. (1996) and Bailey et al. (2000) were developed to extract Sr from the same powders analyzed for carbon isotopes. Approximately 40 mg of powder was pretreated with ultrapure 1M ammonium acetate buffered to a pH of 8 three times (Montanez et al., 1996; Bailey et al., 2000). Samples were then leached in 4% acetic acid (15 minute digestion) and the resulting supernate was collected and spiked with an ^{84}Sr tracer. Sr was isolated using Biorad AG 50X8 cation exchange resin and a 2N HCl based ion exchange. Purified Sr was then loaded with HCl on a Re double-filament configuration. Isotopic compositions were measured using dynamic multicollection with a Finnigan MAT-261A thermal ionization mass spectrometer at the Radiogenic Isotope Laboratory at Ohio State University (Foland and Allen, 1991). The Laboratory value for the SRM 987 standard is ($^{87}Sr/^{86}Sr$) = 0.710242 ±0.000010 (one-sigma external reproducibility). For the $^{87}Sr/^{86}Sr$ values the associated uncertainties given are for two-sigma mean internal reproducibilities. The $^{87}Sr/^{86}Sr$ reported ratios are normalized for instrumental fractionation using a normal Sr ratio of $^{86}Sr/^{88}Sr$ = 0.119400.

Although the methods we use for sample dissolution are designed to minimize leaching of Sr from noncarbonate phases, some amount of contamination is difficult to avoid (Bailey et al., 2000). This characteristically results in increases in the $^{87}Sr/^{86}Sr$ to ratios that are more radiogenic than the initial primary seawater value due in large part to contamination by

radiogenic strontium leached from siliciclastic components (Bailey et al., 2000). Thus, we only utilize the least radiogenic values measured within our section to provide minimum age estimates of critical sample horizons.

Additional References for Sr Methods:

1. Montañez et al., *Geology* **24**, 917 (1996).
2. Bailey et al., *Chem. Geol.* **167**, 313 (2000).
3. Foland and Allen, *Contrib. Mineral. Petrol*. **109**, 195 (1991).

SUPPLEMENTARY FIGURE CAPTIONS

Figure DR1. a: Map showing location of the Confusion Range and Spruce Mountain study areas in the Great Basin, western United States. b: Closer view of study sections.

Figure DR2. Crossplot of $\delta^{13}C_{carb}$ and $\delta^{18}O$ for Confusion Range and Spruce Mountain segments.

Figure DR3. Paleogeographic map modified from Corsetti et al. (2005) showing study area in North America and localities where the latest Permian negative $\delta^{13}C$ excursion is recorded in marine carbonate. Note that localities in which a negative $\delta^{13}C$ excursion is recorded in organic matter only are not plotted here.

Figure DR4. Correlation of the negative $\delta^{13}C_{carb}$ excursion spanning the upper Gerster in the Confusion Range to the sections at Meishan, China (Xie et al. 2007) and Guryul Ravine, Kashmir (Algeo et al., 2007). Also shown are the positions of the Permian-Triassic boundary (PTB), Late Permian Extinction horizon (LPEH), and Late Permian (*praeparvus* zone) sequence boundary (S.B.). Conodont zones used in manuscript Figure 3 are based on $\delta^{13}C_{carb}$ correlation to Guryul Ravine (dashed lines) and where the conodont zones fall with respect to the $\delta^{13}C$ trends.

Figure DR5. $\delta^{13}C_{carb}$ through the late Guadalupian and Lopingian. Data is from Tierney (2010) for Guadalupian and Wuchiapingian, and Korte et al. (2004) for the Changhsingian (composite as plotted in Saltzman and Thomas, 2012). Lower arrow is end-Guadalupian negative $\delta^{13}C_{carb}$ excursion dated to the *xuanhanensis* conodont zone in the Maokou Formation in China (Tierney, 2010; Shen et al., 2007), which may correlate with that documented by Bond et al. (2010) in the *xuanhanensis* zone (although see Isozaki et al., 2007 and Chen et al., 2011 for different curves through this time interval) . This negative $\delta^{13}C$ excursion potentially correlates with the negative excursion we observe in $\delta^{13}C$ in the upper Gerster (manuscript Fig. 2). However, the Sr isotope data do not support this correlation (See discussion in text, Fig. 3, and Fig. DR7). Upper arrow is end-Permian negative $\delta^{13}C_{carb}$ excursion that is discussed in the manuscript text (see also Fig DR4).

Figure DR6. Two time equivalent $\delta^{13}C_{carb}$ curves spanning the late Early Triassic at Zal, Iran and eastern Sichuan Basin, China. Iran data is from Horacek et al. (2007) and Sichuan data from Huang et al. (2012). Stage boundaries are approximate. Upper arrow in both curves is early Olenekian (Smithian) negative $\delta^{13}C_{carb}$ excursion. This negative $\delta^{13}C_{carb}$

excursion potentially correlates with the negative excursion we observe in $\delta^{13}C$ in the upper Gerster (manuscript Fig. 2). However, the Sr isotope data do not support this correlation (See discussion in text, Fig. 3, and Fig. DR7). Note also that the positive $\delta^{13}C_{carb}$ excursion in the Spathian in Iran is smaller magnitude (see also Payne et al 2004) but similar in timing to what we observe in the Thaynes Formation at Spruce Mountain, Nevada (see manuscript Fig. 1). Similar documentation of a large positive $\delta^{13}C$ excursion in the Spathian is observed in China data of Huang et al. (2012). Lower arrow in both curves is end-Permian negative $\delta^{13}C_{carb}$ excursion that is discussed in the manuscript text (see also Fig DR4).

Figure DR7. $^{87}Sr/^{86}Sr$ data in relation to global seawater curve (solid line), modified from Twitchett (2007). This is a close up view of the area shown in manuscript Figure 3 for the latest Triassic through Olenekian (Smithian). Stratigraphic positions of our Confusion Range Sr data are shown in manuscript Fig. 2 (Table S2) and points a through g were assigned to conodont zones indirectly by correlating $\delta^{13}C$ trends in the Confusion Range with the well-dated P-T boundary interval at Guryul Ravine, Pakistan that contains both conodonts and $\delta^{13}C$ (see Fig. DR4, lines of correlation between $\delta^{13}C$ curves in the P-T boundary interval, and S5-S7 for alternative correlations with younger or older excursions in the Tethys). Samples h-i were dated directly to Olenekian (Smithian) zones based on conodonts found at Spruce Mountain (Carr, 1981). Age separation between individual samples within zones (x-axis) is schematic. Dashed lines show two examples of how we use $^{87}Sr/^{86}Sr$ to provide minimum age estimates (see text for discussion). Sample b has an $^{87}Sr/^{86}Sr$ that intersects the seawater curve in the *carinata* zone (vertical dashed line) and thus we assume it can be no younger than this zone and is likely older because of alteration to more radiogenic (higher) values during diagenesis. Based on its absolute $\delta^{13}C$ value and position within the negative excursion (see Fig. DR4), the best age assignment for sample b is latest Permian (horizontal dashed line). Similarly, point e has an $^{87}Sr/^{86}Sr$ that intersects the seawater curve in the late Induan, and its position within the $\delta^{13}C$ minimum (Fig. DR4) suggests an early to middle Induan age. *waagen.=waageni; paskist.=pakistanensis; carina.=carinata; isarci.=isarcica; changxing.-praep.=changxingensis-praeparvus*.

Figure DR8. Permian and Triassic biostratigraphy and geochronology after Henderson et al. (2012) and Ogg (2012) in the The Geologic Time Scale 2012.

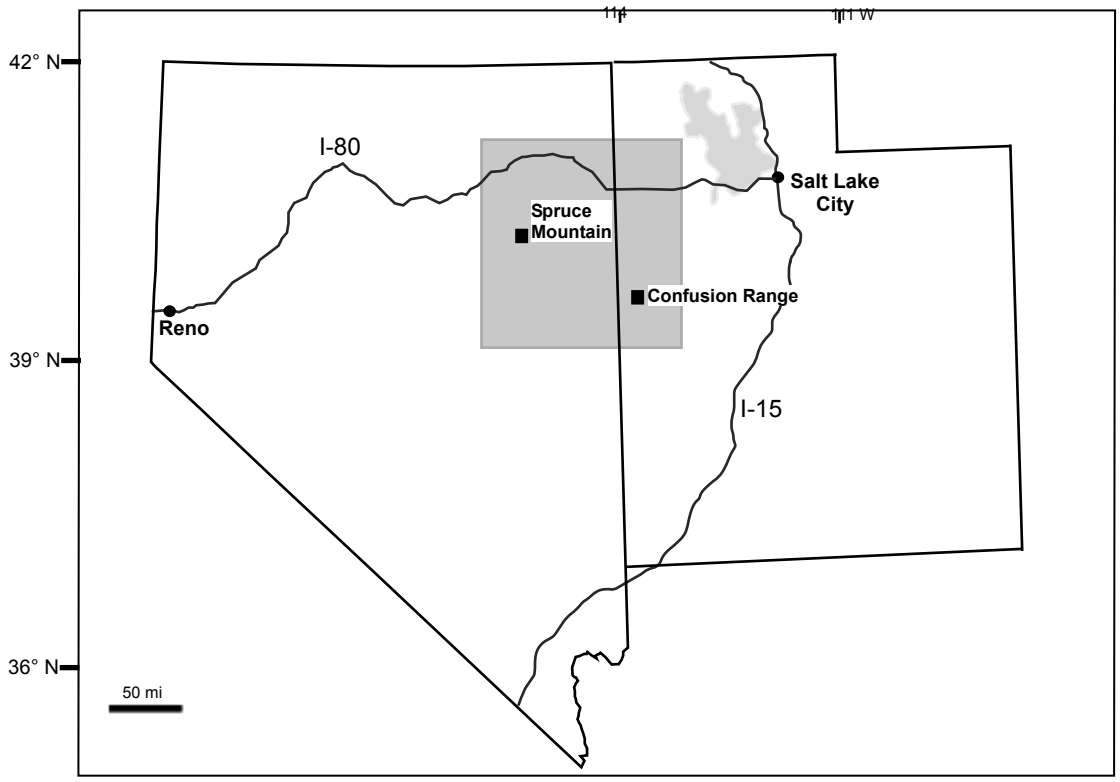

Figure DR1a

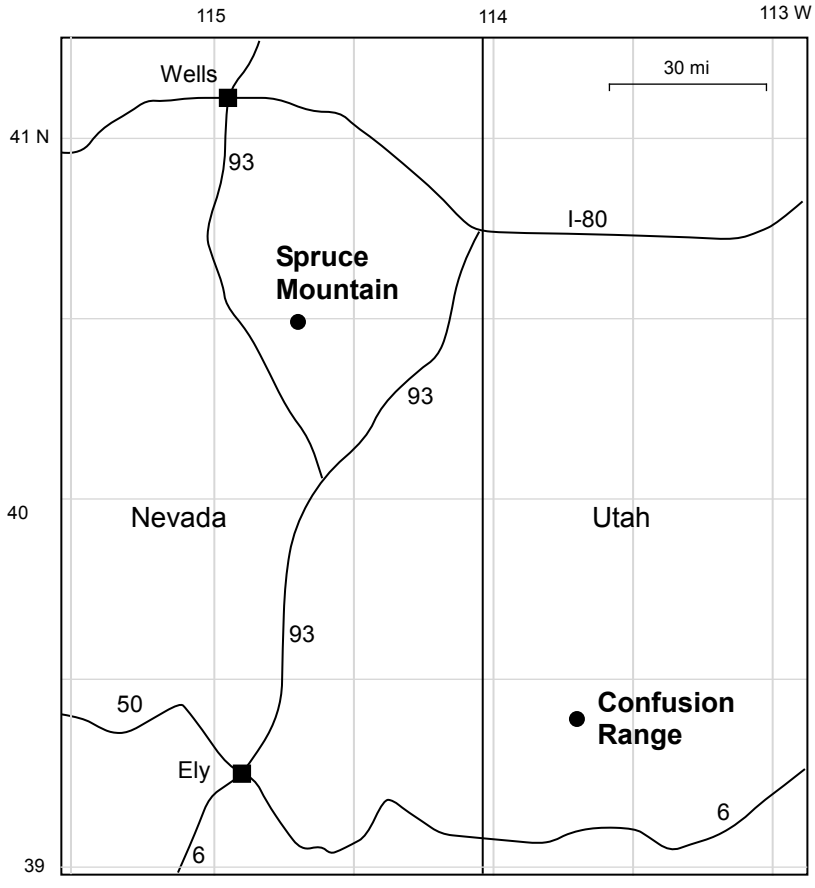

Figure DR1b

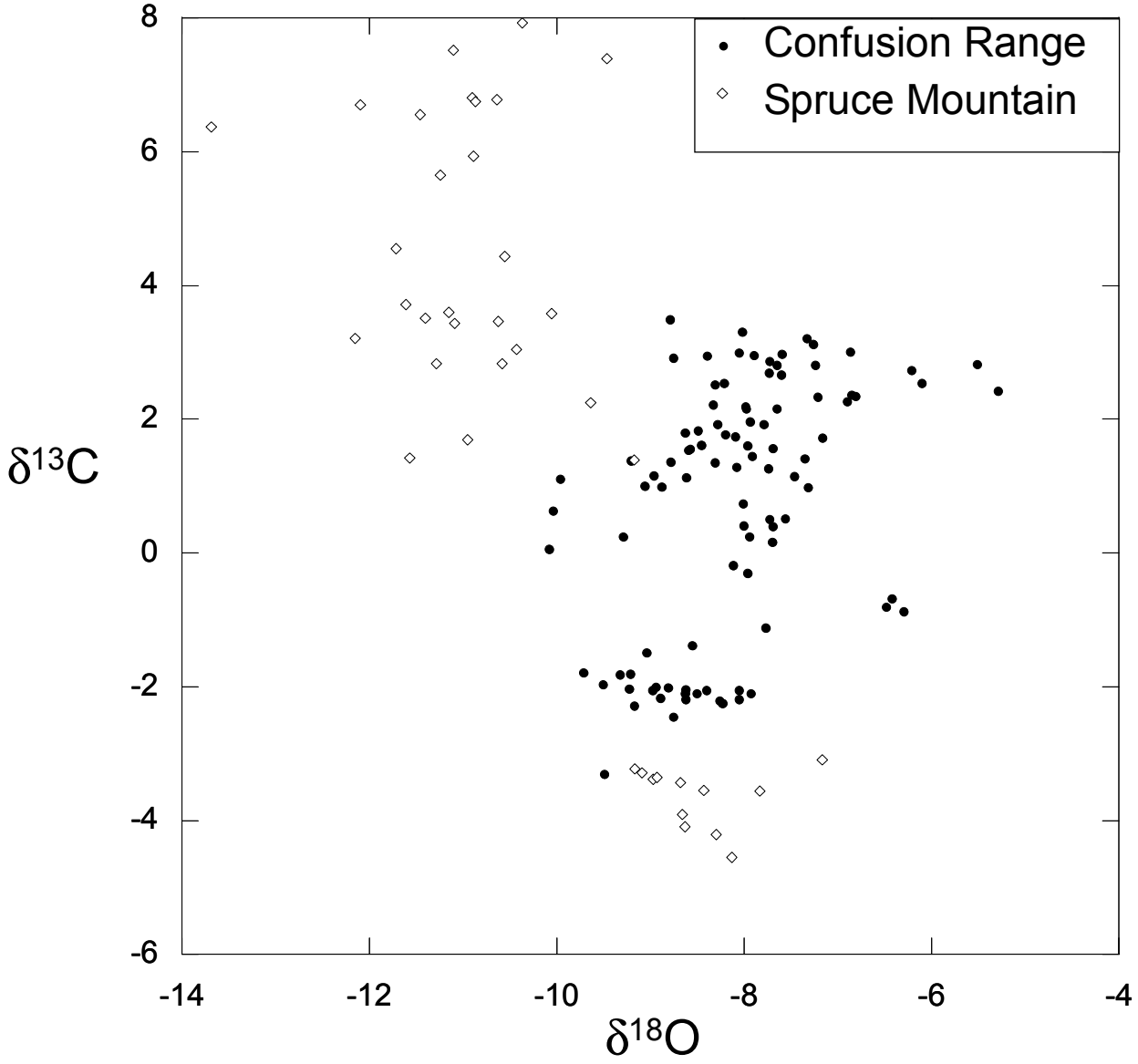
Confusion Range
Spruce Mountain
8
6
4
2
0
-2
-4
-6
-14
-12
-10
-8
-6
-4
δ13C
δ18O

Figure DR2

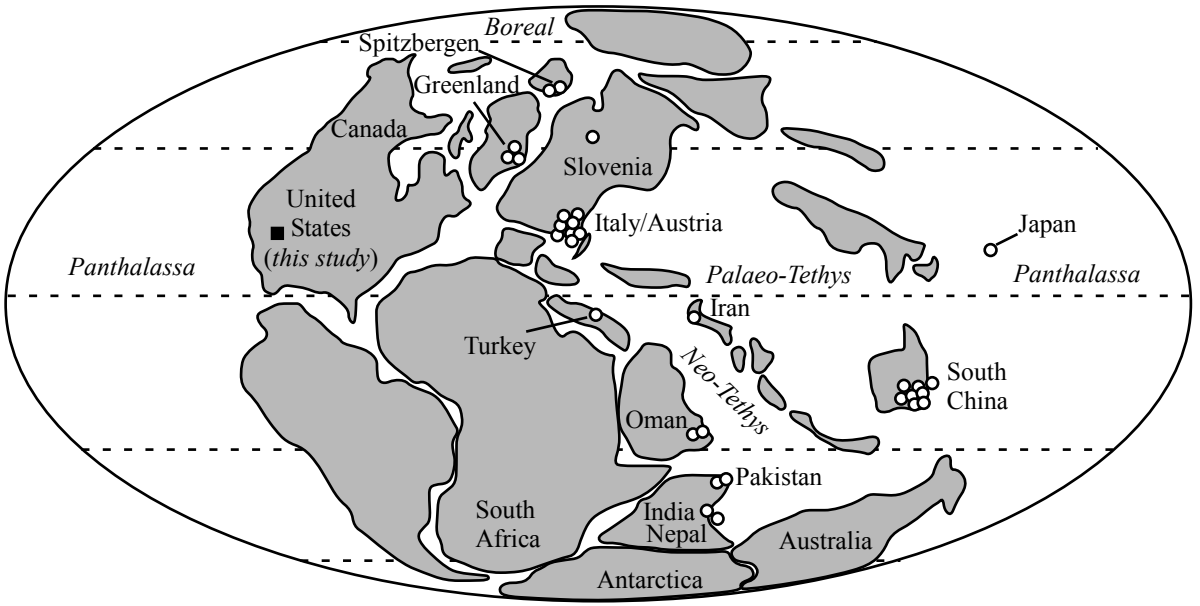
Boreal
Spitzbergen
Greenland
Canada
Slovenia
United
States
(this study)
Italy/Austria
Japan
Panthalassa
Palaeo-Tethys
Panthalassa
Iran
Turkey
Neo-Tethys
South
China
Oman
Pakistan
South
Africa
India
Nepal
Australia
Antarctica

Figure DR3

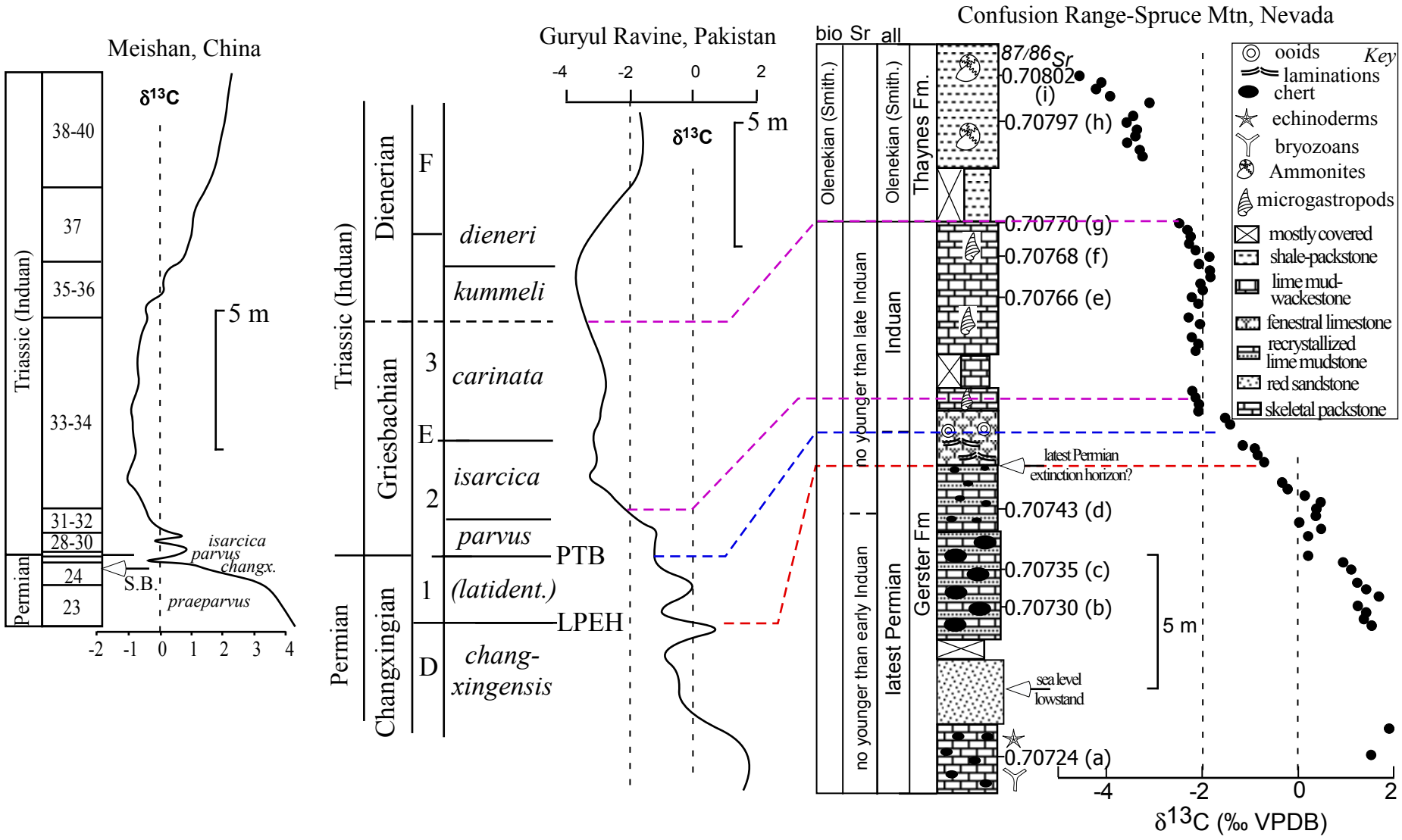
Meishan, China
δ13C
38-40
37
35-36
33-34
31-32
28-30
24
23
Triassic (Induan)
Permian
5 m
S.B.
isarcica
parvus
changx.
praeparvus
-2 -1 0 1 2 3 4
Guryul Ravine, Pakistan
-4 -2 0 2
δ13C
5 m
Triassic (Induan)
Permian
Dienerian
Griesbachian
Changxingian
F
E
3
2
1
D
dieneri
kummeli
carinata
isarcica
parvus
(latident.)
chang-
xingensis
PTB
LPEH
Confusion Range-Spruce Mtn, Nevada
bio Sr all
Olenekian (Smith.)
Olenekian (Smith.)
Thaynes Fm.
no younger than late Induan
no younger than early Induan
Induan
latest Permian
Gerster Fm
87/86Sr
0.70802 (i)
0.70797 (h)
0.70770 (g)
0.70768 (f)
0.70766 (e)
latest Permian extinction horizon?
0.70743 (d)
0.70735 (c)
0.70730 (b)
5 m
sea level lowstand
0.70724 (a)
Key
ooids
laminations
chert
echinoderms
bryozoans
Ammonites
microgastropods
mostly covered
shale-packstone
lime mud-wackestone
fenestral limestone
recrystallized lime mudstone
red sandstone
skeletal packstone
-4 -2 0 2
δ13C (‰ VPDB)

Figure DR4

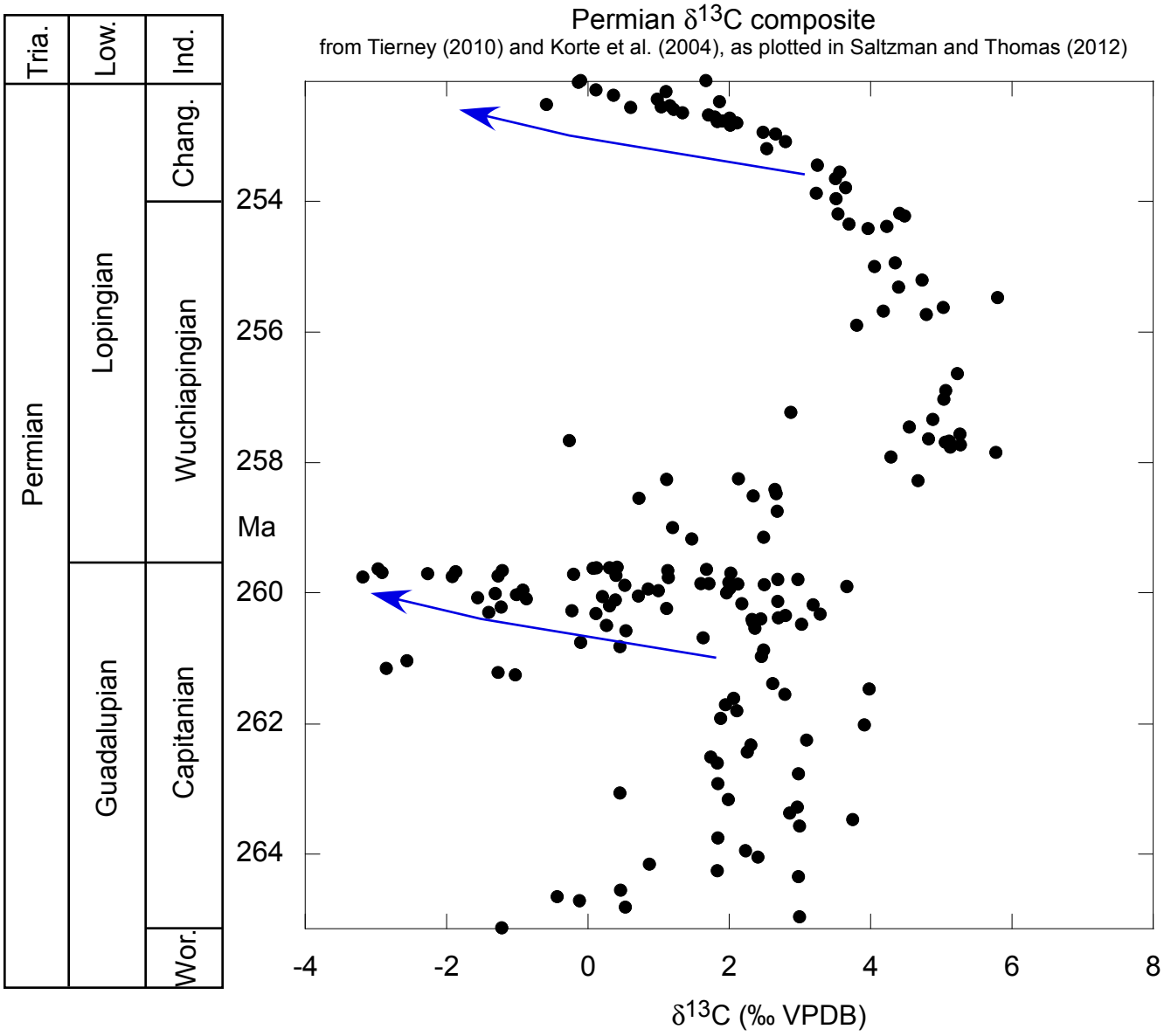
Permian δ13C composite
from Tierney (2010) and Korte et al. (2004), as plotted in Saltzman and Thomas (2012)
Tria.
Low.
Ind.
Permian
Lopingian
Guadalupian
Chang.
Wuchiapingian
Capitanian
Wor.
254
256
258
Ma
260
262
264
-4
-2
0
2
4
6
8
δ13C (‰ VPDB)

Figure DR5

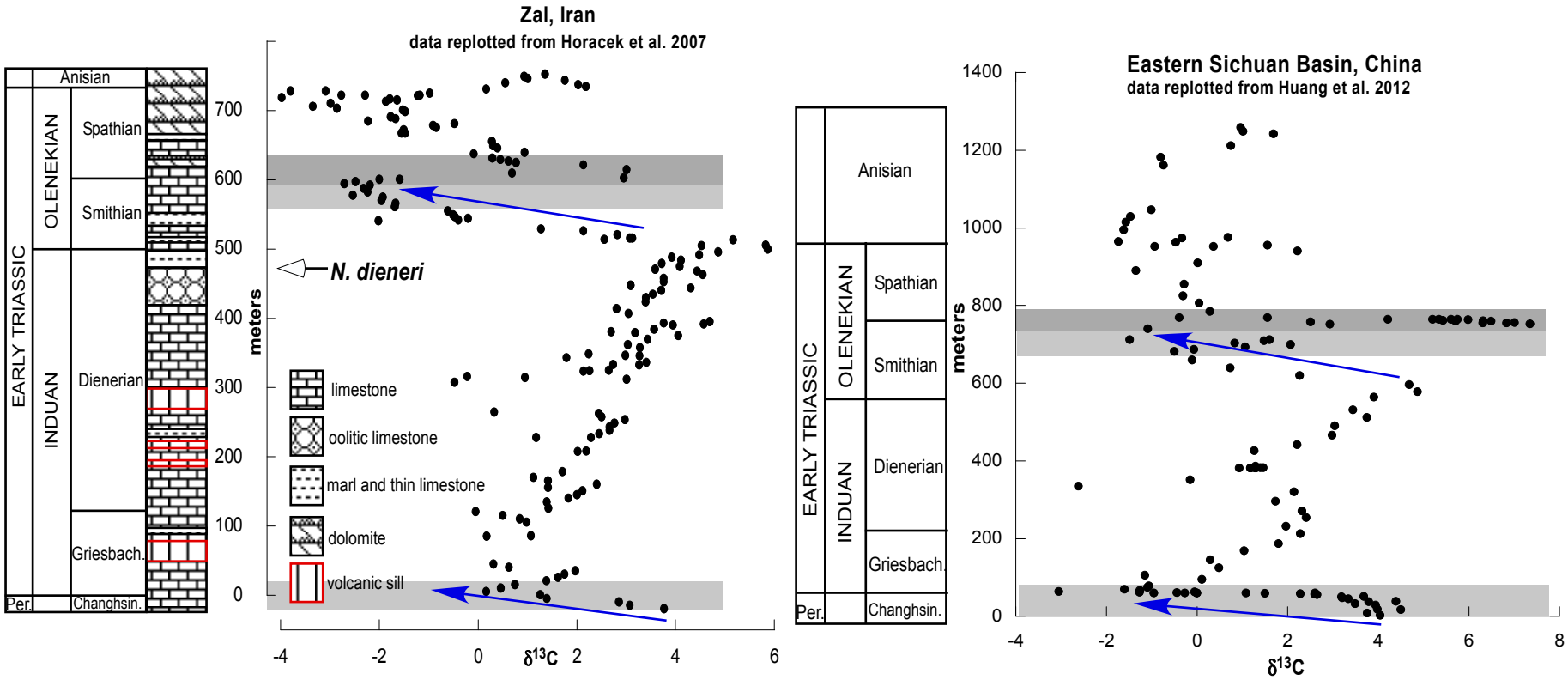
Zal, Iran
data replotted from Horacek et al. 2007
EARLY TRIASSIC
INDUAN
OLENEKIAN
Anisian
Spathian
Smithian
Dienerian
Griesbach.
Changhsin.
Per.
meters
N. dieneri
limestone
oolitic limestone
marl and thin limestone
dolomite
volcanic sill
δ13C
Eastern Sichuan Basin, China
data replotted from Huang et al. 2012

Figure DR6

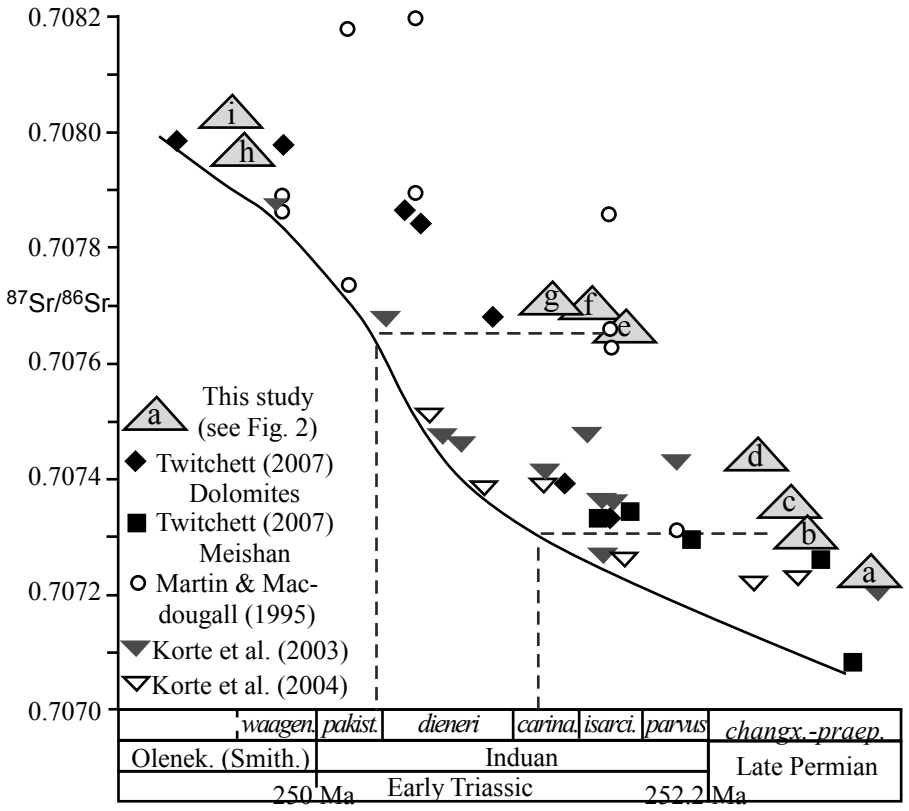
0.7082
0.7080
0.7078
0.7076
0.7074
0.7072
0.7070
87Sr/86Sr
i
h
g
f
e
d
c
b
a
This study
(see Fig. 2)
Twitchett (2007)
Dolomites
Twitchett (2007)
Meishan
Martin & Mac-
dougall (1995)
Korte et al. (2003)
Korte et al. (2004)
waagen.
pakist.
dieneri
carina.
isarci.
parvus
changx.-praep.
Olenek. (Smith.)
Induan
Late Permian
Early Triassic
250 Ma
252.2 Ma

Figure DR7

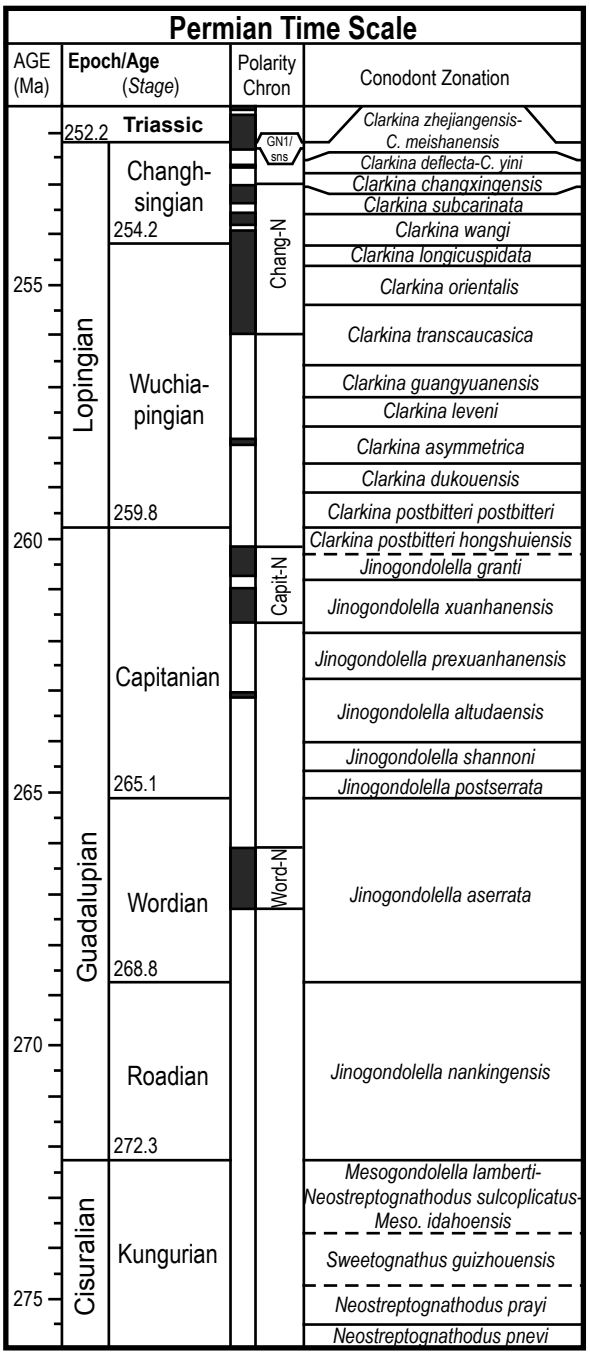
Permian Time Scale
AGE (Ma)
Epoch/Age (Stage)
Polarity Chron
Conodont Zonation
252.2
Triassic
Changh-singian
254.2
Wuchia-pingian
259.8
Capitanian
265.1
Wordian
268.8
Roadian
272.3
Kungurian
Lopingian
Guadalupian
Cisuralian
255
260
265
270
275
GN1/sns
Chang-N
Capit-N
Word-N
Clarkina zhejiangensis-C. meishanensis
Clarkina deflecta-C. yini
Clarkina changxingensis
Clarkina subcarinata
Clarkina wangi
Clarkina longicuspidata
Clarkina orientalis
Clarkina transcaucasica
Clarkina guangyuanensis
Clarkina leveni
Clarkina asymmetrica
Clarkina dukouensis
Clarkina postbitteri postbitteri
Clarkina postbitteri hongshuiensis
Jinogondolella granti
Jinogondolella xuanhanensis
Jinogondolella prexuanhanensis
Jinogondolella altudaensis
Jinogondolella shannoni
Jinogondolella postserrata
Jinogondolella aserrata
Jinogondolella nankingensis
Mesogondolella lamberti-Neostreptognathodus sulcoplicatus-Meso. idahoensis
Sweetognathus guizhouensis
Neostreptognathodus prayi
Neostreptognathodus pnevi

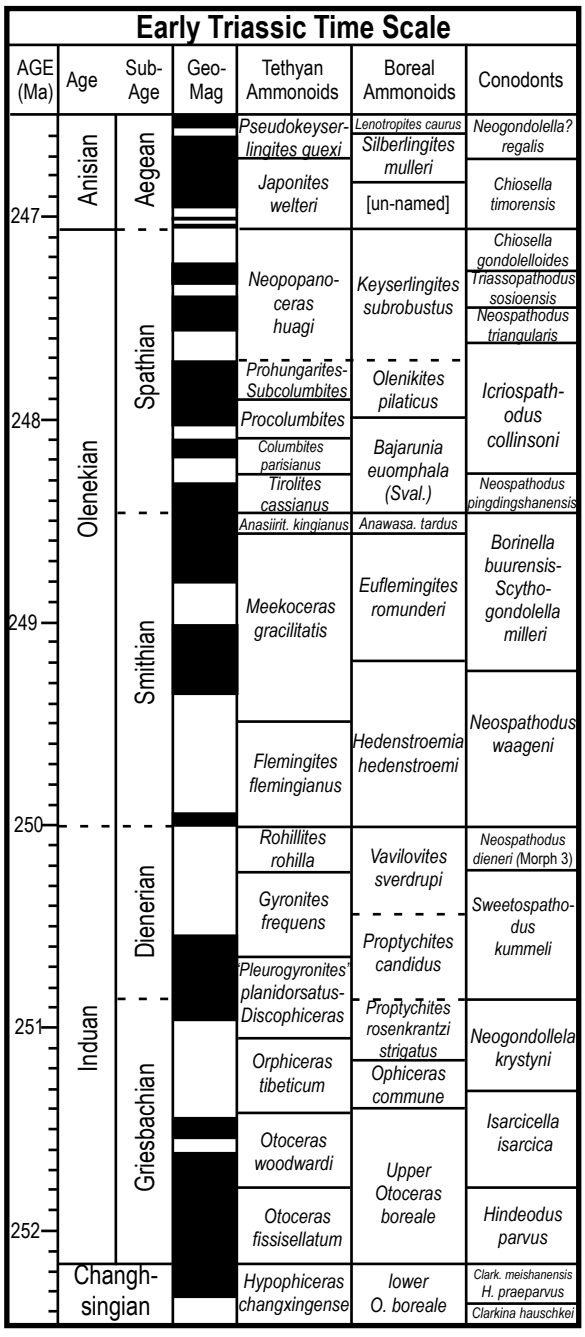
Early Triassic Time Scale
AGE (Ma)
Age
Sub-Age
Geo-Mag
Tethyan Ammonoids
Boreal Ammonoids
Conodonts
Anisian
Olenekian
Induan
Changh-singian
Aegean
Spathian
Smithian
Dienerian
Griesbachian
247
248
249
250
251
252
Pseudokeyser-lingites guexi
Japonites welteri
Neopopano-ceras huagi
Prohungarites-Subcolumbites
Procolumbites
Columbites parisianus
Tirolites cassianus
Anasiirit. kingianus
Meekoceras gracilitatis
Flemingites flemingianus
Rohillites rohilla
Gyronites frequens
'Pleurogyronites' planidorsatus-Discophiceras
Orphiceras tibeticum
Otoceras woodwardi
Otoceras fissisellatum
Hypophiceras changxingense
Lenotropites caurus
Silberlingites mulleri
[un-named]
Keyserlingites subrobustus
Olenikites pilaticus
Bajarunia euomphala (Sval.)
Anawasa. tardus
Euflemingites romunderi
Hedenstroemia hedenstroemi
Vavilovites sverdrupi
Proptychites candidus
Proptychites rosenkrantzi strigatus
Ophiceras commune
Upper Otoceras boreale
lower O. boreale
Neogondolella? regalis
Chiosella timorensis
Chiosella gondolelloides
Triassopathodus sosioensis
Neospathodus triangularis
Icriospath-odus collinsoni
Neospathodus pingdingshanensis
Borinella buurensis-Scytho-gondolella milleri
Neospathodus waageni
Neospathodus dieneri (Morph 3)
Sweetospatho-dus kummeli
Neogondollela krystyni
Isarcicella isarcica
Hindeodus parvus
Clark. meishanensis H. praeparvus
Clarkina hauschkei

Figure DR8

Table DR1. Carbon and Oxygen isotope ratios. Meters are above the base of the Gerster Formation. Complete data set shown in Figure 2. Data shown in Figure 3 are from 215 to 239 meters. Top of Confusion Range section is at 235 meters and remaining samples from Spruce Mountain.

Meters	**$\delta^{13}C$**	**$\delta^{18}O$**
0	3.29	-8.01
12	2.93	-8.38
15	3.47	-8.78
18	3.10	-7.25
21	2.79	-7.64
24	2.67	-7.72
30	2.85	-7.71
36	2.65	-7.59
45	2.34	-6.84
51	2.90	-8.74
66	2.79	-7.23
69	2.97	-8.04
72	2.96	-7.58
81	3.19	-7.32
93	2.94	-7.88
96	2.70	-6.58
99	2.99	-6.85
114	2.52	-8.20
135	2.52	-6.09
138	2.71	-6.20
159	2.40	-5.28
171	2.50	-8.30
177	2.80	-5.50
183	2.32	-6.80
184	1.60	-6.98
185	2.25	-6.89
187	2.14	-7.64
188	1.60	-8.44
190	2.14	-7.96
191	2.31	-7.20
194	2.20	-8.32
196	1.72	-8.08
197	2.17	-7.97
198	1.95	-7.92
199	1.81	-8.48
200	1.33	-8.30
201	1.34	-8.77

202	1.09	-9.95
203	1.11	-8.60
204	0.98	-9.05
205	1.14	-8.95
206	1.75	-8.19
207	1.52	-8.58
208	1.58	-7.95
209	0.97	-8.87
211	1.36	-9.19
212	1.91	-7.78
213	1.78	-8.62
216	1.54	-8.56
217	1.91	-8.27
218	1.55	-7.68
218.25	1.39	-7.34
218.5	1.43	-7.95
218.75	1.26	-8.07
219.1	1.70	-7.15
219.35	1.43	-7.90
219.6	1.25	-7.73
220.1	1.13	-7.45
220.35	0.96	-7.30
220.6	0.22	-9.27
221.35	0.22	-7.93
221.6	0.50	-7.55
221.85	0.04	-10.07
222.1	0.38	-7.68
222.35	0.39	-7.99
222.6	0.49	-7.71
222.85	0.15	-7.68
223.1	-0.20	-8.10
223.35	-0.32	-7.95
224.1	-0.70	-6.41
224.35	-0.83	-6.47
224.6	-0.89	-6.28
224.73	-1.14	-7.76
225.5	-1.40	-8.54
225.75	-1.51	-9.03
226	-2.07	-8.97
226.25	-2.06	-8.61
226.5	-2.12	-8.62

226.75	-2.19	-8.88
228.25	-2.12	-7.92
228.5	-2.07	-8.04
228.75	-2.21	-8.04
229.25	-2.03	-8.80
229.5	-2.27	-8.22
230	-2.07	-8.39
230.25	-2.21	-8.61
230.5	-1.98	-9.49
230.75	-2.02	-8.93
231	-1.81	-9.70
231.25	-1.83	-9.20
231.5	-2.05	-9.21
231.75	-1.84	-9.31
232	-2.12	-8.49
232.25	-2.26	-8.21
232.5	-2.23	-8.25
232.75	-2.30	-9.16
233	-2.47	-8.74
235	-3.33	-9.48
235.5	-3.23	-9.16
235.75	-3.29	-9.09
236	-3.55	-8.43
236.25	-3.38	-8.97
236.5	-3.35	-8.93
236.75	-3.56	-7.83
237	-3.43	-8.68
237.5	-3.09	-7.16
237.75	-3.91	-8.66
238	-4.21	-8.30
238.25	-4.09	-8.63
238.5	-4.55	-8.13
300	3.60	-11.15
301.5	3.21	-12.15
303	3.72	-11.61
306	3.04	-10.43
312	1.42	-11.57
313.5	1.69	-10.95
315	1.39	-9.176
318	2.25	-9.637
319.5	2.83	-10.58

321	3.43	-11.09
325.5	3.57	-10.05
327	3.51	-11.40
328.5	3.46	-10.63
330	2.83	-11.28
336	4.43	-10.55
337.5	4.55	-11.72
340.5	5.65	-11.24
342	5.93	-10.89
343.5	6.55	-11.46
345	6.81	-10.90
346.5	6.70	-12.10
348	6.78	-10.64
349.5	7.52	-11.10
351	7.92	-10.37
354	6.37	-13.69
355.5	6.74	-10.87
357	7.39	-9.47

Table DR2. Strontium isotope ratios. Meters are above the base of the Gerster Formation. See Figure 2 for precise sampling positions. See Figure 3 for comparisons to the seawater curve. Note that samples above 235 m are from Spruce Mountain (see also Table S1), and that although not plotted on Fig. 2, a Sr sample from the top Confusion Range at 235 m is 0.708075 and quite similar to the two values listed at Spruce Mountain for the basal Thaynes.

Meters	**$^{87}Sr/^{86}Sr$**	**Uncertainty (2σ)**	**Sr (ppm)**
238.5	0.708024	0.000006	173.1
236.75	0.707970	0.000014	215.7
233	0.707695	0.000010	172.2
231.75	0.707681	0.000011	88.4
230.25	0.707662	0.000009	94.5
222.35	0.707427	0.000011	99.0
220.1	0.707349	0.000013	117.3
218.75	0.707300	0.000008	98.3
216	0.707237	0.000012	183.6

Additional References for Supplementary Figures:

Algeo, T.J., Hannigan, R., Rowe, H., Brookfield, M., Baud, A., Krystyn, L., and Ellwood, B.B., 2007, Sequencing events across the Permian-Triassic boundary, Guryul Ravine (Kashmir, India). Palaeogeography Palaeoclimatology Palaeoecology, v. 252, p. 328-346.

Chen, B., Joachimski, M.M., Sun, Y., Shen, S., and Lai, X., 2011, Carbon and conodont apatite oxygen isotope records of Guadalupian-Lopingian boundary sections: Climate or sea level signal?: Palaeogeography, Palaeoclimatology, Palaeoecology, v. 311, p. 145–153, doi:10.1016/j.palaeo.2011.08.016.

Corsetti, F.A., Baud, A., Marenco, P.J., and Richoz, S., 2005, Summary of Early Triassic carbon isotope records: Comptes Rendus Palevol, v. 4, p. 473-486.

Henderson, C.M., Davydov, V.I., and Wardlaw, B.R., 2012, The Permian Period, In *A Geologic Time Scale 2012,* eds Gradstein, F., Ogg, J., Schmitz, M., and Ogg, G., Elsevier, p. 653-679.

Horacek, M., Richoz, S., Brandner, R., Krystyn, L., and Spotl, C., 2007, Evidence for recurrent changes in Lower Triassic oceanic circulation of the Tethys: The $\delta^{13}C$ record from marine sections in Iran: Palaeogeography Palaeoclimatotology Palaeoecololology, v. 252, p. 355-369.

Huang, S., Huang, K., Lu, J., and Lan, Y., 2012, Carbon isotopic composition of Early Triassic marine carbonates, Eastern Sichuan Basin, China: Science China Earth Sciences, v. 55, p. 1-13.

Isozaki, Y., Kawahata, H., and Ota, A., 2007, A unique carbon isotope record across the Guadalupian-Lopingian (Middle-Upper Permian) boundary in mid-oceanic paleo-atoll carbonates: The high-productivity "Kamura event" and its collapse in Panthalassa: Global and Planetary Change, v. 55, p. 21-38.

Korte, C., Kozur, H.W., Joachimski, M.M., Strauss, H., Veizer, J., and Schwark, L., 2004, Carbon, sulfur, oxygen, and strontium isotope records, organic geochemistry and biostratigraphy across the Permian/Triassic boundary in Abadeh, Iran: International Journal of Earth Sciences, v. 93, p. 565-581.

Ogg, J., 2012, Triassic, In *A Geologic Time Scale 2012,* eds Gradstein, F., Ogg, J., Schmitz, M., and Ogg, G., Elsevier, p. 681-730.

Payne, J.L., Lehrmann, D.J., Wei, J.Y., Orchard, M.J., Schrag, D.P., and Knoll, A.H., 2004, Large perturbations of the carbon cycle during recovery from the end-Permian extinction: Science, v. 305, p. 506-509.

Saltzman, M.R. and Thomas, E., 2012, Carbon isotope stratigraphy, In *A Geologic Time Scale 2012,* eds Gradstein, F., Ogg, J., Schmitz, M., and Ogg, G., Elsevier, in press.

Shen, S.Z., Wang, Y., Henderson, C.M., Cao, C.Q. Wang, W., 2007. Biostratigraphy and lithofacies of the Permian System in the Laibin-Hshan area of Guangxi, South China. Palaeoworld, v. 16, p. 120-139.

Tierney, K., Permian carbon and strontium isotope stratigraphy in Nevada and China: Implications for a greenhouse-icehouse transition, 2010, unpublished PhD. Ohio State University.

Xie, S., Pancost, R.D., Huang, J., Wignall, P.B., Yu, J., Tang, X., Chen, L., Huang, X., and Lai, X., 2007, Changes in the global carbon cycle occurred as two episodes during the Permian-Triassic crisis: Geology, v. 35, p. 1083–1086.